ACS EARTH AND SPACE CHEMISTRY

Article

Cite This: ACS Earth Space Chem. 2019, 3, 1260−1267

http://pubs.acs.org/journal/aesccq

Multistep Phase Transitions in Sea Surface Microlayer Droplets and Aerosol Mimics using Microfluidic Wells

Lucy Nandy,[†,∥,⊥] Shihao Liu,[†,∥] Connor Gunsbury,[†] Xiaofei Wang,[‡] Matthew A. Pendergraft,[§] Kimberly A. Prather,[‡,§] and Cari S. Dutcher*[,†]

[†]Department of Mechanical Engineering, University of Minnesota, Twin Cities, Minneapolis, Minnesota 55455, United States
[‡]Department of Chemistry and Biochemistry, University of California, San Diego, La Jolla, California 92093, United States
[§]Scripps Institution of Oceanography, University of California, San Diego, La Jolla, California 92093, United States

Supporting Information

ABSTRACT: Oceanic sea spray is one of the largest contributors of atmospheric aerosol particles worldwide. The phase of aerosol particles is known to impact radiative forcing and cloud nucleation. However, as chemically complex aqueous systems that include mixtures of biological, organic, and salt constituents, it is a challenge to predict the phase of sea spray aerosol especially as they age in the atmosphere. In this study, phase behavior (liquid−liquid phase separation, LLPS, and crystallization) of sea surface microlayer (SSML) sample and chemical mimics are investigated using a microfluidic pervaporation approach. Internally mixed aqueous droplets with varying compositions and concentrations are trapped in microfluidic wells, and phase transitions of the droplets are optically determined in a slow dehydration process. A system containing SSML sample combined with an organic acid 3-methyl glutaric acid (3-MGA) undergoes multiple phase changes, including two crystallization and two LLPS events. The added organic acid increases the sample's organic-to-inorganic ratio and moves the system into the range typical of aged SSA. To better understand the contributing constituents to the observed phase changes, control experiments with inorganic salt components NaCl, $MgCl_2$, and Na_2SO_4 are performed with and without 3-MGA, at varying organic to inorganic ratios. 3-MGA leads to LLPS, and the presence of Mg^{2+} more readily facilitates LLPS than Na^+. With the systems studied, LLPS is more prevalent for the chemical mixtures in an intermediate OIR range. This study provides new insight into sea spray aerosol phase as a function of composition and relative humidity and demonstrates multistep phase transitions for these complex systems.

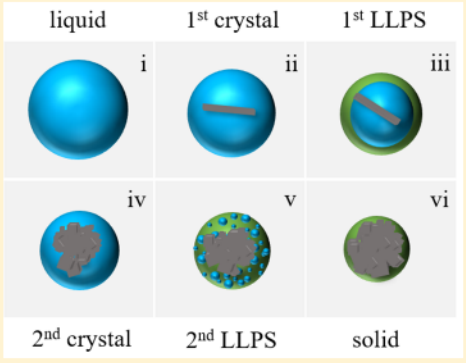

KEYWORDS: *sea spray aerosols, sea surface microlayer, atmospheric aerosols, organic material, droplet microfluidics, liquid−liquid phase separation, crystallization*

1. INTRODUCTION

Sea spray aerosol (SSA) is a major fraction of atmospheric aerosols in coastal and marine environments,[1−3] with important implications for our climate.[4−7] SSA particles are primarily formed when bubbles popping at the sea surface eject nanometer to micrometer sized aqueous droplets that consist of inorganic salts and marine organic material.[7−9] The sea surface microlayer (SSML), the top 1−500 μm of the sea−air interface,[10] is particularly enriched with this surface-active organic matter[11,12] and chemically distinct from the bulk seawater.[13] The SSML is responsible for the presence of a substantial organic fraction in SSA formed by bursting of bubbles.[14−16] The enrichment of organic content has an impact on larger scale atmospheric processes. For example, the number concentration of organic-containing SSA has been shown to affect the cloud formation potential of the aerosols more than particles containing sea salts alone.[5]

In addition to organics, seawater inorganic (e.g., NaCl and $MgCl_2$) and organic (e.g., from organic acids) salts are also a major component in SSA particles, enhancing properties such as water uptake (hygroscopicity) of the particle. Hygroscopic properties for sodium chloride−dicarboxylic acids have been measured using a hygroscopicity tandem differential mobility analyzer (HTDMA) system to study organic matters in SSA, showing hygroscopic dependency on the type of organic acid.[17] Laboratory experiments by Zieger et al.[18] using an HTDMA and an electrodynamic balance (EDB), with artificial seawater (in the absence of organics) and pure sodium chloride aqueous solution, demonstrate that the hygroscopic growth of the aerosol with the salt mix is lower than sodium chloride alone, possibly due to the presence of hydrates (e.g., $MgCl_2{\cdot}6H_2O$ and $CaCl_2{\cdot}6H_2O$) in SSA.[19] Electron microscopy

Special Issue: New Advances in Organic Aerosol Chemistry

Received: May 1, 2019
Revised: June 10, 2019
Accepted: June 12, 2019
Published: June 12, 2019

DOI: 10.1021/acsearthspacechem.9b00121
ACS Earth Space Chem. 2019, 3, 1260−1267

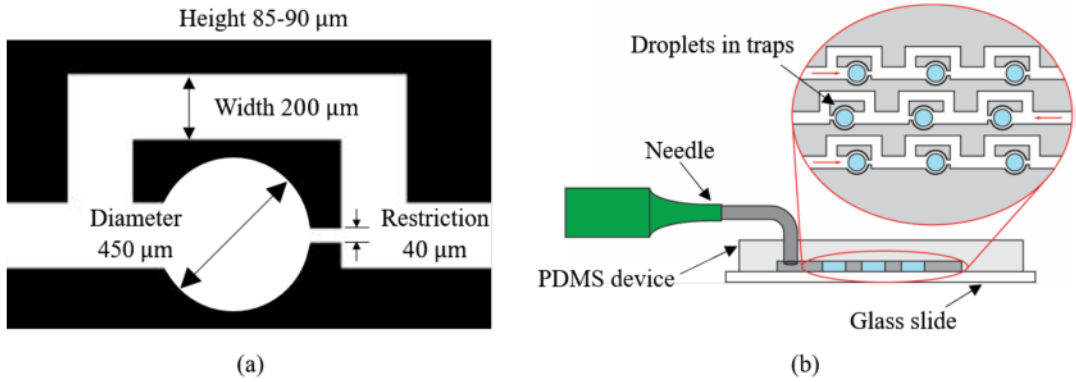

Figure 1. (a) Microfluidic well in the device fabricated with soft lithography. The heights of all the wells are within 85−90 μm. The exact height of each well is measured with surface profilometer. (b) Schematic of trapped droplets in microfluidic wells (side view and enlarged top view). The droplets are surrounded by silicone oil, resulting in a thin lubrication layer of oil near the upper and bottom walls.

and X-ray spectromicroscopy analysis of NaCl particles mixed with organic acids[20] reveal the formation of organic salts that impact the chemical composition and hygroscopic and optical properties of aged particles due to reactivity of SSA with secondary organics upon drying.

The unique inorganic−organic composition of SSA can lead to particles of varied phase, depending on atmospheric temperature and relative humidity. In addition to liquid (deliquesced) and solid (crystallized) phases, liquid−liquid phase separation (LLPS) may also occur in these mixed ion−organic systems during atmospheric humidity cycles.[21] LLPS is often caused by the salting-out effect, which reduces the solubility of the organic compound with increase in the salt mole fraction in the solution. Recent laboratory studies to investigate morphological changes have shown the sea salt particles undergo phase events such as LLPS at low relative humidity (RH).[22] An experimental study[23] using laser mass spectrometry shows evidence of the presence of organics mostly internally mixed in SSA. However, since the precise chemical composition of SSA is uncertain, comprehensively linking chemical composition to climate relevant properties is yet to be achieved.[24] Additional laboratory studies by use of cryogenic transmission electron microscopy (cryo-TEM) demonstrate structural and chemical changes in SSA with varying environmental conditions.[25] Mixing state exhibiting core−shell morphology of aerosol particles containing NaCl and glucose has been quantified by measuring the organic volume fraction using atomic force microscopy (AFM) and high-performance liquid chromatography (HPLC) techniques.[26] Besides LLPS, efflorescence of mixed particles is also dictated by the interactions between salts and organic matter. Varying organic−inorganic ratios (OIRs) of the mixtures can alter the separation relative humidity (SRH) as well as the efflorescence relative humidity (ERH),[27] which leads to a variety of aerosol particle phases (liquid, solid, LLPS, and viscous phase states[28]), with a significant impact on gas-to-particle partitioning.[29]

The composition, phase, and mixing state of SSA result in distinct impacts on cloud condensation nucleation (CCN). In a laboratory study, Altaf et al. showed that liquid−liquid phase separated systems have elevated levels of CCN activity, compared to well mixed particles of the same composition.[30] Additionally, varied chemical compositions influences the particle mixing state, whether they are external mixtures or their corresponding equivalent internal mixtures, therefore impacting the CCN activity.[31] Global simulations performed using the general circulation model have shown that sea salt emissions increase the CCN concentrations.[32] Global aerosol model simulations to study the influence of organics in SSA on CCN concentrations[33] show that the organics decrease the surface tension of CCN, enabling CCN activation and increasing the cloud droplet number concentration, significantly influencing the cloud albedo.[34]

Important insights into aerosol particle phase and hygroscopicity have been obtained through laboratory study on both aerosol samples and model chemical systems. For example, Estillore et al.[35] have measured the hygroscopicity and studied the surface microstructure by AFM imaging, for model systems containing mixtures of sugars and inorganic salts, and laboratory-generated SSA samples in order to examine the impact of organics and morphology on the SSA growth factor. The authors found that particles containing water-soluble organics such as marine carbohydrates led to gradual deliquescence, therefore growing more in size upon hydration than particles containing sodium halides that deliquesce spontaneously. This continuous growth in pure organics leads to the same gradual hydration behavior in phase-separated particles with an organic coating. Additionally, we have used a microfluidic approach to study the aerosol droplet phase of $(NH_4)_2SO_4$ containing aqueous organic mixtures,[36] which have composition similar to those of aerosol particles from anthropogenic sources. Droplets are trapped in microfluidic wells, and the high permeability of poly(dimethylsiloxane) (PDMS; the channel material) to water allows slow dehydration of droplets. In due course, phase transitions such as LLPS and crystallization can be observed when the relative humidity reaches corresponding critical values.

Here we employ the microfluidic approach to SSML samples collected from a seawater mesocosm,[37] to further advance understanding of SSA hygroscopicity and phase as a function of chemical composition. Both environmental samples and complex model systems containing organic acids, sea salts, and laboratory-produced SSML are investigated. In addition, synthetic seawater (SSW) droplets, with and without an added organic acid, are studied to observe LLPS and crystallization. The effects of the major salt components of SSML on the phase transitions are discussed in terms of the number and concentration of the solutes in SSML on the microfluidic platform. This work demonstrates that multiple

DOI: 10.1021/acsearthspacechem.9b00121
ACS Earth Space Chem. 2019, 3, 1260−1267

Table 1. Systems Studied, Organic-to-Inorganic Ratios (OIRs), and Phase Transitions

salt	organic	OIR (by dry mass)	phase transition
SSML	–	[a]	crystallization
SSML	3-MGA	[a]	crystallization−LLPS−crystallization−LLPS
SSW	3-MGA	1.39	crystallization−LLPS−crystallization−LLPS
NaCl	–	–	crystallization
NaCl	3-MGA	1	crystallization
$NaCl + MgCl_2$	–	–	crystallization
$NaCl + MgCl_2$	3-MGA	1.31	crystallization−LLPS
$NaCl + MgCl_2$	3-MGA	1.68	LLPS−crystallization−LLPS
$NaCl + MgCl_2$	3-MGA	1.86	LLPS−crystallization−LLPS
$NaCl + MgCl_2$	3-MGA	2.52	crystallization−LLPS
$NaCl + MgCl_2 + Na_2SO_4$	–	–	crystallization
$NaCl + MgCl_2 + Na_2SO_4$	3-MGA	1.48	LLPS−crystallization−LLPS

[a]Value unavailable.

phase state transitions occur in SSML in the presence of an added organic acid and systematically explores how different salts contribute to each of the transitions and resulting internal structure.

2. EXPERIMENTAL METHOD AND SOLUTION PREPARATION

A microfluidic platform is used to study LLPS and efflorescence phase behavior of droplets containing organic and inorganic mixtures. The device is made of PDMS (Sylgard 184 Silicone Elastomer, Dow Corning Corp.) on a wafer with the molded microfluidic channels. The geometry of the channel (Figure 1a) is designed in a computer-aided design (CAD) based software, Draftsight (Dassault Systèmes), printed on a mask by CAD/Art Services, Inc., and fabricated on a silicon wafer using soft lithography techniques.[38,39] After wafer fabrication, the height of the channel is measured with a surface profilometer. Then PDMS is poured over the wafer, degassed, and cured at 75 °C, and each individual chip is cut out from the wafer. Holes are punched at the inlet and outlet of the device for all individual chips and cleaned using a plasma cleaner. Finally, the PDMS device is sealed on a glass cover slide and baked in the oven at 75 °C for over 2 h.

Once the microfluidic chip is complete, silicone oil (Sigma-Aldrich, CAS Reg. No. 63148-62-9) is injected into the device using tight syringes (Hamilton) to remove air. The sample is then loaded with a pressure high enough to overcome the capillary pressure at the well restriction, completely filling the device with the test solution. Silicone oil is again injected, removing all of the test solution that is outside the wells. What remains is a droplet of sample in each well surrounded by oil. The schematic of the trapped droplets in microfluidic wells is shown in Figure 1b. The droplets remain trapped in the microfluidic wells under laboratory ambient conditions (23 °C, 18−25% RH). Due to the permeability of PDMS to water and the low RH outside the device, volumes of the trapped droplets reduce with time as the water content decreases. The water first diffuses through the lubrication oil separating the droplets and the PDMS wells and then permeates out of the device through the PDMS material. The increase in solute concentration leads to changes in phase, observed optically. An inverted microscope (Olympus CKX53) and Lumenera INFINITY2-2 M (mono) camera are used to capture the images of the dehydration process every 10 s. The reported images in this study are processed by ImageJ and MATLAB to crop images and calculate the scale bar.

Microfluidic trap pervaporation experiments are performed with SSML sample, with and without 3-methyl glutaric acid (3-MGA; Tokyo Chemical Industry, CAS Reg. No. 0626-51-7). The SSML was sampled from 400 L of seawater collected from Ellen Browning Scripps Memorial Pier at Scripps Institution of Oceanography on Sep. 25, 2017 at 11 AM. The seawater is placed in a plastic drum outside, exposed to sunlight, and phytoplankton growth medium at the f/50 level is added (see *Culture of Phytoplankton for Feeding Marine Invertebrates* by Robert R. L. Guillard;[40] Aquatic Eco-Systems Inc., Apopka, FL, USA). The SSML was sampled on Sep. 27, 2017 using the glass plate method[10] and stored frozen.

For the chemical mimic systems, sodium chloride (NaCl; Fisher Scientific, CAS Reg. No. 7647-14-5), magnesium chloride hexahydrate ($MgCl_2 \cdot 6H_2O$; Research Products International Corp., CAS Reg. No. 7791-18-6), and sodium sulfate (Na_2SO_4; Fisher Scientific, CAS Reg. No. 7757-82-6) are used as the inorganic components. An atmospherically relevant dicarboxylic acid,[41,42] 3-MGA, is used as the organic component since it is present in both primary marine aerosols (from enrichment in the SSML),[43] as well as in secondary marine organic aerosols (e.g., from olefin oxidation).[44−46] The solutes are dissolved in HPLC-grade water (Fisher Scientific, CAS Reg. No. 7732-18-5) to make mixture solutions for the phase study. On adding the organic acid to the system, the sample's OIR (by dry mass) increases and moves the system into the range of OIRs typical of SSA (typically 1−4,[47−49] after aging). The concentration of binary 3-MGA solution for all experiments is fixed at 50 mg/mL, and the concentration of binary NaCl is 50 mg/mL. Salt solutions with at least two components are set at an inorganic mass ratio consistent with the standard ASTM D1141-98 for sea salt mix (https://www.syntheticseawater.com/products/sea-salt-astm-d1141-98). The salt and organic solutions are then mixed to achieve the targeted OIR, by dry mass for each experiment. This study also uses synthetic seawater (SSW; Ricca Chemical Co., R8363000, ASTM D1141 substitute ocean water without heavy metals or organics), with and without 3-MGA. For the systems used to mimic phase transitions observed for 3-MGA + SSML droplet, the SSW is mixed with 3-MGA with the volume ratio 1:1, the same as the one used for the 3-MGA + SSML system. A summary of all of the studied systems, with OIRs and observed phase transitions, are reported in Table 1.

DOI: 10.1021/acsearthspacechem.9b00121
ACS Earth Space Chem. 2019, 3, 1260−1267

3. RESULTS AND DISCUSSION

Crystallization, with the appearance of a possible liquid organic coating, is observed for the SSML sample (Figure 2a).

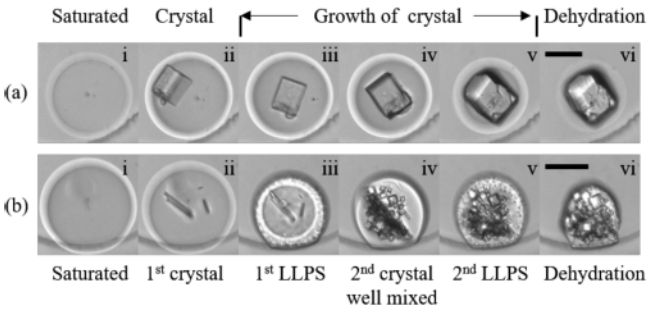

Figure 2. (a) Phase transitions observed in SSML: bright-field images of the solution droplet; time span (from i to vi), ~1 h; scale bar, 50 μm. (b) Phase transitions observed in 3-MGA + SSML aqueous solution (50% by volume, 50 mg/mL 3-MGA; 50% by volume, SSML): bright-field images of the solution droplet; time span (from i to vi), ~4 h; scale bar, 50 μm.

Although the dissolved organic carbon (DOC) was not measured for the SSML samples, typically they contain 100–200 μmol/L (μM) DOC.[50,51] A cubic crystal nucleates and grows while the droplet continues to dehydrate as water leaves the droplet through the PDMS device. However, by adding a single organic acid (here, 3-MGA) to the SSML sample to increase the organic content, *two* crystallization and *two* LLPS events occur (Figure 2b). Initially, the droplet becomes supersaturated and a crystal nucleates (Figure 2b(ii)), followed by the first LLPS event (Figure 2b(iii)). Here, the organic phase appears to coat the inner aqueous salt-rich phase. A second crystallization is then observed (Figure 2b(iv)), where many small cubic crystals are formed, and the liquid phase once again becomes well-mixed, likely due to the sudden reduction in the ionic strength of the aqueous phase. Finally, the second LLPS (Figure 2b(v)) occurs after the second crystallization and remains in this phase for the remaining droplet dehydration process. This multistep phase transition is also shown in Supporting Information Video S1.

Simplified chemical mimic systems are then used to determine the key constituents for the multiple step transitions observed in the 3-MGA + SSML system. The contribution from the largely insoluble long-chain organic and biological components in SSML is first excluded by using SSW. Using the same mixing volume ratio of 3-MGA:SSW as 3-MGA:SSML, the same phase behavior results are observed (Figure 3), which indicates the insignificance of biological components to the particular quaternary phase change sequence (crystallization–LLPS–crystallization–LLPS). While the effect of insoluble long-chain organic and biological components in the mimic system can be ignored, SSW itself contains 10 salts. To further illuminate the role of the individual salts, the main salt components of SSW (NaCl, $MgCl_2$, and Na_2SO_4) are separately studied with and without water-soluble 3-MGA.

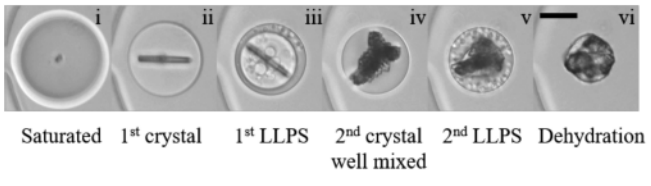

Figure 3. Phase transitions observed in 3-MGA + SSW aqueous solution (50% by volume, 50 mg/mL 3-MGA; 50% by volume, SSW; OIR ≈ 1.39 by dry mass): bright-field images of the solution droplet; time span (from i to vi), ~4.5 h; scale bar, 50 μm.

NaCl is the most abundant inorganic component in seawater (58.5% of the sea salt mix by mass). Aqueous NaCl solution droplets undergo efflorescence (homogeneous nucleation of a salt crystal) at a water activity of 0.44, equivalent in the atmosphere to a gas-phase RH of 44%.[52,53] For the binary water + NaCl experiments shown here, cubic NaCl crystal results as expected with dehydration as shown in Figure 4a.

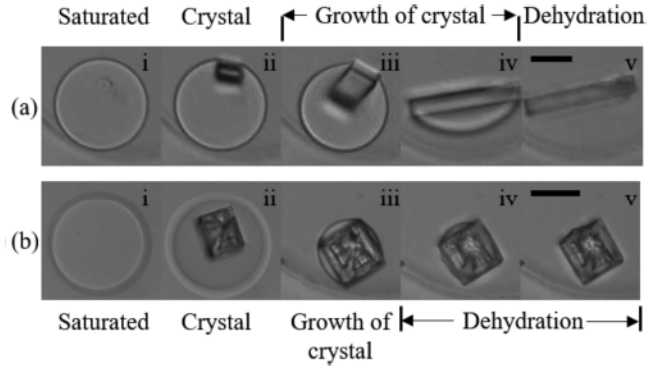

Figure 4. (a) Phase transitions observed in binary NaCl aqueous solution (50 mg/mL): bright-field images of the solution droplet; time span (from ii to v), ~3 h; scale bar, 50 μm. (b) Phase transitions observed in ternary 3-MGA + NaCl aqueous solution (50% by volume, 50 mg/mL 3-MGA; 50% by volume, 50 mg/mL NaCl; OIR = 1 by dry mass): bright-field images of the solution droplet; time span (from i to v), ~21 h; scale bar, 50 μm.

Next, 3-MGA is added to the NaCl system, with a 1:1 dry mass solute ratio, yet no liquid–liquid phase separation is observed (Figure 4b). Instead, a crystal forms, with a modified appearance presumably due to the formation of organic salts surrounding the cubic-shaped NaCl core.[20] The crystal continues to grow while the droplet dehydrates completely. It is worth noting that the crystal structure is similar in appearance to that shown with the pure SSML samples in Figure 2a. A similar phenomenon is also observed for OIRs from 1.84 to 3.40 for 3-MGA + NaCl aqueous systems.

In order to observe LLPS, the second most abundant salt component of seawater by mass, $MgCl_2$ (12.4% of sea salt mix), is added to the NaCl solution with a mass ratio same as the standard sea salt mix. Divalent cations, such as that in $MgCl_2$, have been found to ionically facilitate coadsorption of soluble organic matter to SSML, subsequently increasing the organic concentration in SSA.[54] In addition, compared to monovalent cations, Mg^{2+} has been found by Wu et al.[55] to facilitate the occurrence of LLPS in mixtures containing glutaric acid. For experiments with the ternary NaCl + $MgCl_2$ solution, efflorescence is again observed (Figure 5a), with the crystal growth continuing until the droplet completely dehydrates. When 3-MGA is added to the ternary salt solution, LLPS appears as the first phase transition (Figure 5b(ii)). At low enough water content, salt in the aqueous core crystallizes, which decreases the ionic strength of the remaining aqueous phase. This allows for the remixing of the two liquid phases into one well-mixed phase (Figure 5b(iii)), similar to that observed with the 3-MGA + SSML system in Figure 2b.

DOI: 10.1021/acsearthspacechem.9b00121
ACS Earth Space Chem. 2019, 3, 1260–1267

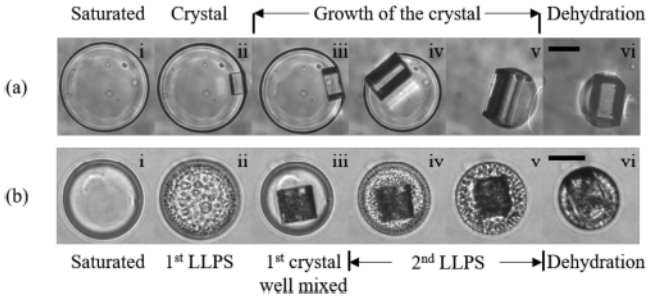

Figure 5. (a) Phase transitions observed in NaCl + $MgCl_2$ (24.53 mg/mL NaCl; 5.20 mg/mL $MgCl_2$) aqueous salt mixture: bright-field images of the solution droplet; time span (from i to vi), ~3 h. (b) Phase transitions observed in 3-MGA + NaCl + $MgCl_2$ aqueous solution (50% by volume, 50 mg/mL 3-MGA; 50% by volume, salt mixture; OIR = 1.68 by dry mass): bright-field images of the solution droplet; time span (from i to vi), ~1.2 h; scale bar, 50 μm.

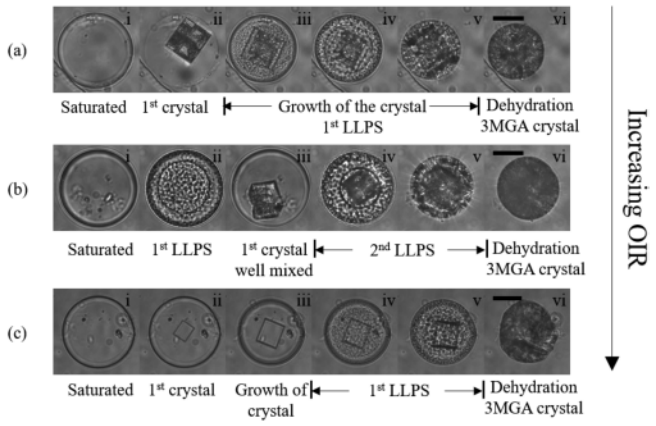

Figure 6. Phase transitions observed in 3-MGA + NaCl + $MgCl_2$ aqueous solution by mixing 50 mg/mL 3-MGA and 24.53 mg/mL NaCl + 5.20 mg/mL $MgCl_2$ aqueous salt mixture with different volume ratios corresponding to distinct OIRs by dry mass: bright-field images of the solution droplet; scale bar, 50 μm; OIR, (a) 1.31, (b) 1.86, and (c) 2.52; time span (from i to vi), (a) ~3.2, (b) ~2, and (c) ~1 h.

Likewise, a second LLPS event is observed with the 3-MGA + NaCl + $MgCl_2$ system (Figure 5b(iv,v)), similar to Figure 2b(v) with further dehydration, highlighting the importance of $MgCl_2$ in the droplet phase equilibrium. This second LLPS may be explained by two contributions. One contribution is the ultralow efflorescence point of $MgCl_2$, meaning dissolved $MgCl_2$ remains present in the aqueous solution at extremely low RH,[56] enabling a second liquid−liquid phase separation before $MgCl_2$ has a chance to crystallize. Another complementary contribution is that the divalent Mg^{2+} facilitates LLPS of salt solution and 3-MGA more readily compared to monovalent cations,[55,57] such as Na^+, which also explains the absence of LLPS for the 3-MGA + NaCl system.

Although many similarities are found between the 3-MGA + NaCl + $MgCl_2$ system and the 3-MGA-SSML system, a key difference is that the first phase transition seen in the SSML and SSW systems is crystallization, which is not observed in the 3-MGA + NaCl + $MgCl_2$ system. Rather, a liquid−liquid phase separation occurs first. To consider the potential effects of OIR on the efflorescence and separation relative humidities, and order of phase transitions, the OIR, by dry mass of 3-MGA + NaCl + $MgCl_2$ is varied by changing the mixing volume ratio of 3-MGA to the fixed two-salt mix. Multiple possible transitions are observed (Figure 6), with two critical OIRs for the first transition type, and subsequent phase change order of this quaternary system is found.

The mixing state of aerosol particles generally depends on the OIR,[36,58,59] and for the SSA in particular, the OIR varies between 1 and 4.[47−49] Starting at a relatively high inorganic salt content with OIR of 1.31 (Figure 6a), crystallization is observed first (Figure 6a(ii)). The crystal gradually grows; then a LLPS occurs. Note that only one LLPS takes place in the experiment, because only one salt remains after the first crystallization. As the organic content increases, for OIR = 1.68 and 1.86, LLPS is observed first (Figure 5b(ii) and Figure 6b(ii), respectively), likely indicating enough 3-MGA is salted out to form a phase before the efflorescence relative humidity of one salt, presumably NaCl, is reached. After crystallization (Figure 5b(iii) and Figure 6b(iii)), a second LLPS is observed (Figure 5b(iv,v) and Figure 6b(iv,v)), though, again, no second crystallization. As OIR is increased further to 2.52 (Figure 6c), efflorescence and LLPS change their order in the dynamic phase change process again. This is similar to that observed for the 3-MGA + $(NH_4)_2SO_4$ system,[36] where it was found that while having more organic typically promotes the occurrence of LLPS, at high enough organic content, LLPS is suppressed. While Figure 6 demonstrates a few possible transitions, only one crystallization event occurs for all OIRs tested for the 3-MGA + NaCl + $MgCl_2$ system. Arguably, this is also because of the low ERH of $MgCl_2$,[56] which only crystallizes in aqueous systems at extremely low water content.

In order to attempt to mimic the observed 3-MGA + SSML system phase transitions, it is clear that at least three salts are needed in the mixture solution. Na_2SO_4, the third most abundant salt component of the SSW (9.8% of sea salt mix by mass), has a higher ERH than NaCl[60] and is possibly one of the crystals observed for the 3-MGA + SSML and 3-MGA + SSW systems. Therefore, Na_2SO_4 is added to the NaCl + $MgCl_2$ and 3-MGA + NaCl + $MgCl_2$ systems, at the same salt ratio mix as SSW. The NaCl + $MgCl_2$ + Na_2SO_4 system without added 3-MGA only shows the crystallization of the salts (Figure 7a), as expected. With the organic acid added, a surprising three-phase LLPS is observed for the 3-MGA + NaCl + $MgCl_2$ + Na_2SO_4 system (Figure 7b(ii)). The evolution of this three-phase LLPS is elaborated in Figure 7c and Supporting Information Video S2. The droplet (Figure 7c(iii)) shows diffusion of molecules at the beginning of the phase transition, which forms a two-phase LLPS (Figure 7c(iv)). Then, another two-phase LLPS starts in the inner phase of the droplet, forming what appears to be a three-phase LLPS (Figure 7c(v)) state. Alternatively, perhaps the state is a two-phase double emulsion system with the composition of the innermost phase the same as the outermost shell. Next, when one phase, presumably the NaCl-rich aqueous phase, becomes concentrated enough, it forms the first crystal observed in this experiment (Figure 7b(iii),c(vii)), accompanied by the possible remixing of the other two phases (labeled as "well-mixed" in the figures). Then a two-phase LLPS (Figure 7b(iv,v)) and further crystallization (Figure 7b(vii)) of the inner phase are shown. One possible reason for a first transition of LLPS instead of crystallization as seen in 3-MGA + SSW and 3-MGA + SSML is that Na_2SO_4 also strongly salts out organics,[61] similar to $MgCl_2$, due to the valency of the sulfate ion. It may be that the first crystallization can only be seen when there are enough numbers of monovalent ions in

DOI: 10.1021/acsearthspacechem.9b00121
ACS Earth Space Chem. 2019, 3, 1260−1267

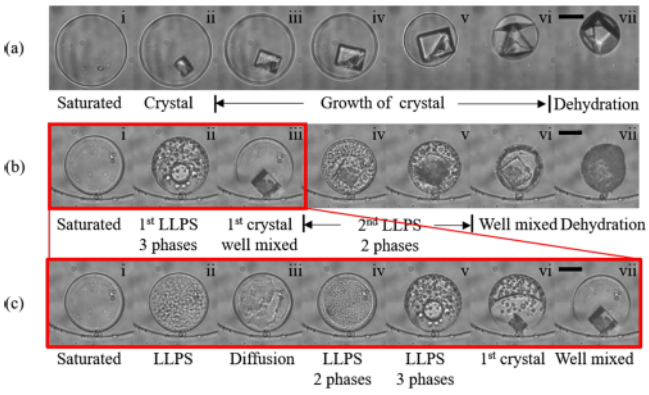

Figure 7. (a) Phase transitions observed in NaCl + $MgCl_2$ + Na_2SO_4 (24.53 mg/mL NaCl; 5.20 mg/mL $MgCl_2$; 4.09 mg/mL Na_2SO_4) aqueous salt mixture: bright-field images of the solution droplet; time span (from i to vii), ∼4 h; scale bar, 50 μm. (b) Phase transitions observed in 3-MGA + NaCl + $MgCl_2$ + Na_2SO_4 aqueous solution (50% by volume, 50 mg/mL 3-MGA; 50% by volume, aqueous salt mixture; OIR = 1.48 by dry mass): bright-field images of the solution droplet; time span (from i to vii), ∼2 h; scale bar, 50 μm. (c) Higher time resolution images of the same experiment as that in panel b, representing evolution of the three-phase LLPS (b(i) to b(iii)): bright-field images of the solution droplet; time span (from i to vii), ∼14 min; scale bar, 50 μm.

the solutions, beyond those included here. The complex interactions among the different salts and the organic acid, while not fully understood, certainly impact the ERH and SRH of the mixtures.

4. CONCLUSIONS

A multistep crystallization−LLPS−crystallization−LLPS transition pathway was observed for the first time for both 3-MGA + SSML and 3-MGA + SSW. A portion of the multistep transition, LLPS−crystallization−LLPS, was successfully repeated with 3-MGA + NaCl + $MgCl_2$ droplets. Additional mimic systems containing 3-MGA along with three sea salts were studied, resulting in further complex phase observations, including a surprising three-phase LLPS and two remixing steps. The first crystallization step observed in 3-MGA + SSML and 3-MGA + SSW, however, was not observed for the three salt systems. Future work should entail additional salts and OIRs, as well as a study of the impact of other key components found in the SSML such as the biological and largely insoluble long-chain organic carbons on phase, to more accurately model SSA chemical complexity.

Sea spray aerosol is abundant in the atmosphere, yet the impact of the chemical complexity on cloud properties is not fully understood. It is vital to study the mixing state of sea salt and organic mixtures to understand the fundamental aerosol properties controlling cloud activation. This work highlights different phase states of collected SSML samples; it also separates the main sea salts in the samples to study the contribution of each salt to the observed phase and internal heterogeneities using a microfluidic platform. The work highlights the complexity of the interactions among different salts and an organic acid, affecting ERH and SRH, as well as the number of transition pathways possible. The effect of the solute concentrations on the phase behavior studied here continues to emphasize the importance of OIR to the aerosol particles−providing insight into the changing phase of sea spray generated aerosols in the atmosphere with changing relative humidities.

■ ASSOCIATED CONTENT

Supporting Information

The Supporting Information is available free of charge on the ACS Publications website at DOI: 10.1021/acsearthspacechem.9b00121.

Video of evaporation of 50 mg/mL 3-methyl glutaric acid−sea surface microlayer (SSML) aqueous solution droplet with volume ratio 1:1 in a microfluidic well, from Figure 2b (AVI)

Video of three-phase liquid separation in 3-MGA + NaCl + $MgCl_2$ + Na_2SO_4 aqueous system with OIR = 1.48 by dry mass, from Figure 7c (AVI)

■ AUTHOR INFORMATION

Corresponding Author

*E-mail: cdutcher@umn.edu. Tel.: 612-624-0428.

ORCID

Lucy Nandy: 0000-0001-7647-9837

Cari S. Dutcher: 0000-0003-4325-9197

Present Address

[⊥]Department of Atmospheric Sciences, University of Illinois at Urbana−Champaign, Urbana, IL 61801.

Author Contributions

[∥]L.N. and S.L. contributed equally to this work.

Notes

The authors declare no competing financial interest.

■ ACKNOWLEDGMENTS

This material is based upon work supported in part by the National Science Foundation under NSF CAREER Grant No. 1554936, including the measurements and analysis of the laboratory chemical mimic systems. This work was also supported by NSF through the NSF Center for Aerosol Impacts on Chemistry of the Environment (NSF-CAICE) under Grant No. CHE-1801971, including the sampling and measurements of the environmental SSML samples. Portions of this work were conducted in the Minnesota Nano Center, which is supported by the National Science Foundation through the National Nano Coordinated Infrastructure Network (NNCI) under Award No. ECCS-1542202.

■ REFERENCES

(1) Seinfeld, J. H.; Pandis, S. N. *Atmospheric Chemistry and Physics, from Air Pollution to Climate Change*; John Wiley: New York, 1998.

(2) Finlayson-Pitts, B. J. The Tropospheric Chemistry of Sea Salt: A Molecular-Level View of the Chemistry of NaCl and NaBr. *Chem. Rev.* **2003**, *103* (12), 4801−4822.

(3) Grythe, H.; Ström, J.; Krejci, R.; Quinn, P.; Stohl, A. A Review of Sea-Spray Aerosol Source Functions Using a Large Global Set of Sea Salt Aerosol Concentration Measurements. *Atmos. Chem. Phys.* **2014**, *14* (3), 1277−1297.

(4) Haywood, J.; Boucher, O. Estimates of the Direct and Indirect Radiative Forcing Due to Tropospheric Aerosols: A Review. *Rev. Geophys.* **2000**, *38* (4), 513−543.

(5) de Leeuw, G.; Andreas, E. L.; Anguelova, M. D.; Fairall, C. W.; Lewis, E. R.; O'Dowd, C.; Schulz, M.; Schwartz, S. E. Production Flux of Sea-Spray Aerosol. *Rev. Geophys.* **2011**, *49* (2), 1−39.

(6) Murphy, D. M.; Anderson, J. R.; Quinn, P. K.; McInnes, L. M.; Brechtel, F. J.; Kreidenweis, S. M.; Middlebrook, A. M.; Posfai, M.;

Thomson, D. S.; Buseck, P. R. Influence of Sea-Salt on Aerosol Radiative Properties in the Southern Ocean Marine Boundary Layer. *Nature* **1998**, *392*, 62−65.
(7) Tseng, R.-S.; Viechnicki, J. T.; Skop, R. A.; Brown, J. W. Sea-to-Air Transfer of Surface-Active Organic Compounds by Bursting Bubbles. *J. Geophys. Res.* **1992**, *97* (C4), 5201−5206.
(8) Brown, J. W.; Skop, R. A.; Viechnicki, J.; Tseng, R.-S. Transport of Surface-Active Organic Materials from Seawater to the Air-Water Interface by an Ascending Current Field. *Fluid Dyn. Res.* **1992**, *9* (1−3), 97−105.
(9) Blanchard, D. C. Bubble Scavenging and the Water-to-Air Transfer of Organic Material in the Sea. *Adv. Chem. Ser.* **1975**, *145* (145), 360−387.
(10) Cunliffe, M.; Engel, A.; Frka, S.; Gašparović, B. Ž.; Guitart, C.; Murrell, J. C.; Salter, M.; Stolle, C.; Upstill-Goddard, R.; Wurl, O. Sea Surface Microlayers: A Unified Physicochemical and Biological Perspective of the Air-Ocean Interface. *Prog. Oceanogr.* **2013**, *109* (2013), 104−116.
(11) Liss, P.; Duce, R. *The Sea Surface and Global Change*; Cambridge University Press: Cambridge, U.K., 1997.
(12) Blanchard, D. C. Sea-to-Air Transport of Surface Active Material. *Science (Washington, DC, U. S.)* **1964**, *146* (3642), 396−397.
(13) Zhang, Z.; Liu, L.; Liu, C.; Cai, W. Studies on the Sea Surface Microlayer: II. The Layer of Sudden Change of Physical and Chemical Properties. *J. Colloid Interface Sci.* **2003**, *264* (1), 148−159.
(14) Gantt, B.; Meskhidze, N. The Physical and Chemical Characteristics of Marine Primary Organic Aerosol: A Review. *Atmos. Chem. Phys.* **2013**, *13* (8), 3979−3996.
(15) Russell, L. M.; Hawkins, L. N.; Frossard, A. A.; Quinn, P. K.; Bates, T. S. Carbohydrate-like Composition of Submicron Atmospheric Particles and Their Production from Ocean Bubble Bursting. *Proc. Natl. Acad. Sci. U. S. A.* **2010**, *107* (15), 6652−6657.
(16) Quinn, P. K.; Bates, T. S.; Schulz, K. S.; Coffman, D. J.; Frossard, A. A.; Russell, L. M.; Keene, W. C.; Kieber, D. J. Contribution of Sea Surface Carbon Pool to Organic Matter Enrichment in Sea Spray Aerosol. *Nat. Geosci.* **2014**, *7* (3), 228−232.
(17) Peng, C.; Jing, B.; Guo, Y. C.; Zhang, Y. H.; Ge, M. F. Hygroscopic Behavior of Multicomponent Aerosols Involving NaCl and Dicarboxylic Acids. *J. Phys. Chem. A* **2016**, *120* (7), 1029−1038.
(18) Zieger, P.; Väisänen, O.; Corbin, J. C.; Partridge, D. G.; Bastelberger, S.; Mousavi-Fard, M.; Rosati, B.; Gysel, M.; Krieger, U. K.; Leck, C. Revising the Hygroscopicity of Inorganic Sea Salt Particles. *Nat. Commun.* **2017**, *8*, No. 15883, DOI: 10.1038/ncomms15883.
(19) Wexler, A. S.; Seinfeld, J. H. Second-Generation Inorganic Aerosol Model. *Atmos. Environ., Part A* **1991**, *25* (12), 2731−2748.
(20) Laskin, A.; Moffet, R. C.; Gilles, M. K.; Fast, J. D.; Zaveri, R. A.; Wang, B.; Nigge, P.; Shutthanandan, J. Tropospheric Chemistry of Internally Mixed Sea Salt and Organic Particles: Surprising Reactivity of NaCl with Weak Organic Acids. *J. Geophys. Res. Atmos.* **2012**, *117*, D15302.
(21) Marcolli, C.; Krieger, U. K. Phase Changes during Hygroscopic Cycles of Mixed Organic/Inorganic Model Systems of Tropospheric Aerosols. *J. Phys. Chem. A* **2006**, *110* (5), 1881−1893.
(22) Patterson, J. P.; Collins, D. B.; Michaud, J. M.; Axson, J. L.; Sultana, C. M.; Moser, T.; Dommer, A. C.; Conner, J.; Grassian, V. H.; Stokes, M. D.; et al. Sea Spray Aerosol Structure and Composition Using Cryogenic Transmission Electron Microscopy. *ACS Cent. Sci.* **2016**, *2* (1), 40−47.
(23) Middlebrook, A. M.; Murphy, D. M.; Thomson, D. S. Observations of Organic Material in Individual Marine Particles at Cape Grim during the First Aerosol Characterization Experiment (ACE 1). *J. Geophys. Res.* **1998**, *103* (D13), 16475−16483.
(24) Tsigaridis, K.; Koch, D.; Menon, S. Uncertainties and Importance of Sea Spray Composition on Aerosol Direct and Indirect Effects. *J. Geophys. Res. Atmos.* **2013**, *118* (1), 220−235.
(25) Patterson, J. P.; Collins, D. B.; Michaud, J. M.; Axson, J. L.; Sultana, C. M.; Moser, T.; Dommer, A. C.; Conner, J.; Grassian, V. H.; Stokes, M. D.; et al. Sea Spray Aerosol Structure and Composition Using Cryogenic Transmission Electron Microscopy. *ACS Cent. Sci.* **2016**, *2* (1), 40−47.
(26) Lee, H. D.; Kaluarachchi, C. P.; Hasenecz, E. S.; Zhu, J. Z.; Popa, E.; Stone, E. A.; Tivanski, A. V. Effect of Dry or Wet Substrate Deposition on the Organic Volume Fraction of Core-Shell Aerosol Particles. *Atmos. Meas. Tech.* **2019**, *12*, 2033−2042.
(27) Bertram, A. K.; Martin, S. T.; Hanna, S. J.; Smith, M. L.; Bodsworth, A.; Chen, Q.; Kuwata, M.; Liu, A.; You, Y.; Zorn, S. R. Predicting the Relative Humidities of Liquid-Liquid Phase Separation, Efflorescence, and Deliquescence of Mixed Particles of Ammonium Sulfate, Organic Material, and Water Using the Organic-to-Sulfate Mass Ratio of the Particle and the Oxygen-to-Carbon Ele. *Atmos. Chem. Phys.* **2011**, *11* (21), 10995−11006.
(28) Slade, J. H.; Ault, A. P.; Bui, A. T.; Ditto, J. C.; Lei, Z.; Bondy, A. L.; Olson, N. E.; Cook, R. D.; Desrochers, S. J.; Harvey, R. M.; et al. Bouncier Particles at Night: Biogenic Secondary Organic Aerosol Chemistry and Sulfate Drive Diel Variations in the Aerosol Phase in a Mixed Forest. *Environ. Sci. Technol.* **2019**, *53*, 4977−4987.
(29) Erdakos, G. B.; Pankow, J. F. Gas/Particle Partitioning of Neutral and Ionizing Compounds to Single- and Multi-Phase Aerosol Particles. 2. Phase Separation in Liquid Particulate Matter Containing Both Polar and Low-Polarity Organic Compounds. *Atmos. Environ.* **2004**, *38* (7), 1005−1013.
(30) Altaf, M. B.; Dutcher, D. D.; Raymond, T. M.; Freedman, M. A. Effect of Particle Morphology on Cloud Condensation Nuclei Activity. *ACS Earth Sp. Chem.* **2018**, *2* (6), 634−639.
(31) Schill, S. R.; Collins, D. B.; Lee, C.; Morris, H. S.; Novak, G. A.; Prather, K. A.; Quinn, P. K.; Sultana, C. M.; Tivanski, A. V.; Zimmermann, K.; et al. The Impact of Aerosol Particle Mixing State on the Hygroscopicity of Sea Spray Aerosol. *ACS Cent. Sci.* **2015**, *1* (3), 132−141.
(32) Pierce, J. R.; Adams, P. J. Global Evaluation of CCN Formation by Direct Emission of Sea Salt and Growth of Ultrafine Sea Salt. *J. Geophys. Res.* **2006**, *111* (6), 1−16.
(33) Westervelt, D. M.; Moore, R. H.; Nenes, A.; Adams, P. J. Effect of Primary Organic Sea Spray Emissions on Cloud Condensation Nuclei Concentrations. *Atmos. Chem. Phys.* **2012**, *12* (1), 89−101.
(34) O'Dowd, C. D.; Facchini, M. C.; Cavalli, F.; Ceburnis, D.; Mircea, M.; Decesari, S.; Fuzzi, S.; Yoon, Y. J.; Putaud, J. Biogenically Driven Organic Contribution to Marine Aerosol. *Nature* **2004**, *431*, 676−680.
(35) Estillore, A. D.; Morris, H. S.; Or, V. W.; Lee, H. D.; Alves, M. R.; Marciano, M. A.; Laskina, O.; Qin, Z.; Tivanski, A. V.; Grassian, V. H. Linking Hygroscopicity and the Surface Microstructure of Model Inorganic Salts, Simple and Complex Carbohydrates, and Authentic Sea Spray Aerosol Particles. *Phys. Chem. Chem. Phys.* **2017**, *19* (31), 21101−21111.
(36) Nandy, L.; Dutcher, C. S. Phase Behavior of Ammonium Sulfate with Organic Acid Solutions in Aqueous Aerosol Mimics Using Microfluidic Traps. *J. Phys. Chem. B* **2018**, *122*, 3480−3490.
(37) Prather, K. A.; Bertram, T. H.; Grassian, V. H.; Deane, G. B.; Stokes, M. D.; DeMott, P. J.; Aluwihare, L. I.; Palenik, B. P.; Azam, F.; Seinfeld, J. H.; et al. Bringing the Ocean into the Laboratory to Probe the Chemical Complexity of Sea Spray Aerosol. *Proc. Natl. Acad. Sci. U. S. A.* **2013**, *110* (19), 7550−7555.
(38) McDonald, J. C.; Duffy, D. C.; Anderson, J. R.; Chiu, D. T.; Wu, H.; Schueller, O. J. A.; Whitesides, G. M. Review General Fabrication of Microfluidic Systems in Poly(Dimethylsiloxane). *Electrophoresis* **2000**, *21*, 27−40.
(39) Qin, D.; Xia, Y.; Whitesides, G. M. Soft Lithography for Micro- and Nanoscale Patterning. *Nat. Protoc.* **2010**, *5* (3), 491−502.
(40) *Culture of Marine Invertebrate Animals*; Smith, W. L., Chanley, M. H., Eds.; Plenum Press: New York and London, 1975.
(41) Saxena, P.; Hildemann, L. M. Water-Soluble Organics in Atmospheric Particles: A Critical Review of the Literature and Application of Thermodynamics to Identify Candidate Compounds. *J. Atmos. Chem.* **1996**, *24* (1), 57−109.

DOI: 10.1021/acsearthspacechem.9b00121
ACS Earth Space Chem. 2019, 3, 1260−1267

(42) Chebbi, A.; Carlier, P. Carboxylic Acids in the Troposphere, Occurrence, Sources, and Sinks: A Review. *Atmos. Environ.* **1996**, *30* (24), 4233−4249.
(43) Carlson, D. J. Dissolved Organic Materials in Surface Microlayers: Temporal and Spatial Variability and Relation to Sea State. *Limnol. Oceanogr.* **1983**, *28* (3), 415−431.
(44) Turekian, V. C. Concentrations, Isotopic Compositions, and Sources of Size-Resolved, Particulate Organic Carbon and Oxalate in near-Surface Marine Air at Bermuda during Spring. *J. Geophys. Res.* **2003**, *108* (D5), 4157.
(45) Losey, D. J.; Parker, R. G.; Freedman, M. A. PH Dependence of Liquid-Liquid Phase Separation in Organic Aerosol. *J. Phys. Chem. Lett.* **2016**, *7* (19), 3861−3865.
(46) Cochran, R. E.; Laskina, O.; Jayarathne, T.; Laskin, A.; Laskin, J.; Lin, P.; Sultana, C.; Lee, C.; Moore, K. A.; Cappa, C. D.; et al. Analysis of Organic Anionic Surfactants in Fine and Coarse Fractions of Freshly Emitted Sea Spray Aerosol. *Environ. Sci. Technol.* **2016**, *50* (5), 2477−2486.
(47) Keene, W. C.; Maring, H.; Maben, J. R.; Kieber, D. J.; Pszenny, A. A. P.; Dahl, E. E.; Izaguirre, M. A.; Davis, A. J.; Long, M. S.; Zhou, X.; et al. Chemical and Physical Characteristics of Nascent Aerosols Produced by Bursting Bubbles at a Model Air-Sea Interface. *J. Geophys. Res.* **2007**, *112* (21), 1−16.
(48) Laskina, O.; Morris, H. S.; Grandquist, J. R.; Qin, Z.; Stone, E. A.; Tivanski, A. V.; Grassian, V. H. Size Matters in the Water Uptake and Hygroscopic Growth of Atmospherically Relevant Multi-component Aerosol Particles. *J. Phys. Chem. A* **2015**, *119* (19), 4489−4497.
(49) Cochran, R. E.; Ryder, O. S.; Grassian, V. H.; Prather, K. A. Sea Spray Aerosol: The Chemical Link between the Oceans, Atmosphere, and Climate. *Acc. Chem. Res.* **2017**, *50* (3), 599−604.
(50) Engel, A.; Sperling, M.; Sun, C.; Grosse, J.; Friedrichs, G. Organic Matter in the Surface Microlayer: Insights From a Wind Wave Channel Experiment. *Front. Mar. Sci.* **2018**, *5*, 2296−7745.
(51) Wilson, T. W.; Ladino, L. A.; Alpert, P. A.; Breckels, M. N.; Brooks, I. M.; Browse, J.; Burrows, S. M.; Carslaw, K. S.; Huffman, J. A.; Judd, C.; et al. A Marine Biogenic Source of Atmospheric Ice-Nucleating Particles. *Nature* **2015**, *525* (7568), 234−238.
(52) Koop, T.; Kapilashrami, A.; Molina, L. T.; Molina, M. J. Phase Transitions of Sea-Salt/Water Mixtures at Low Temperatures: Implications for Ozone Chemistry in the Polar Marine Boundary Layer. *J. Geophys. Res.* **2000**, *105* (D21), 26393−26402.
(53) Tang, I. N. Chemical and Size Effects of Hygroscopic Aerosols on Light Scattering Coefficients. *J. Geophys. Res. Atmos.* **1996**, *101* (D14), 19245−19250.
(54) Schill, S. R.; Burrows, S. M.; Hasenecz, E. S.; Stone, E. A.; Bertram, T. H. The Impact of Divalent Cations on the Enrichment of Soluble Saccharides in Primary Sea Spray Aerosol. *Atmosphere* **2018**, *9* (12), 476.
(55) Wu, F. M.; Wang, X. W.; Jing, B.; Zhang, Y. H.; Ge, M. F. Liquid-Liquid Phase Separation in Internally Mixed Magnesium Sulfate/Glutaric Acid Particles. *Atmos. Environ.* **2018**, *178*, 286−292.
(56) Gupta, D.; Eom, H. J.; Cho, H. R.; Ro, C. U. Hygroscopic Behavior of NaCl-$MgCl_2$ Mixture Particles as Nascent Sea-Spray Aerosol Surrogates and Observation of Efflorescence during Humidification. *Atmos. Chem. Phys.* **2015**, *15* (19), 11273−11290.
(57) Görgényi, M.; Dewulf, J.; Van Langenhove, H.; Héberger, K. Aqueous Salting-out Effect of Inorganic Cations and Anions on Non-Electrolytes. *Chemosphere* **2006**, *65* (5), 802−810.
(58) Song, M.; Marcolli, C.; Krieger, U. K.; Zuend, A.; Peter, T. Liquid-Liquid Phase Separation in Aerosol Particles: Dependence on O:C, Organic Functionalities, and Compositional Complexity. *Geophys. Res. Lett.* **2012**, *39* (19), L19801.
(59) Stewart, D. J.; Cai, C.; Nayler, J.; Preston, T. C.; Reid, J. P.; Krieger, U. K.; Marcolli, C.; Zhang, Y. H. Liquid-Liquid Phase Separation in Mixed Organic/Inorganic Single Aqueous Aerosol Droplets. *J. Phys. Chem. A* **2015**, *119* (18), 4177−4190.
(60) Gao, Y.; Yu, L. E.; Chen, S. B. Efflorescence Relative Humidity of Mixed Sodium Chloride and Sodium Sulfate Particles. *J. Phys. Chem. A* **2007**, *111* (42), 10660−10666.
(61) Riva, M.; Chen, Y.; Zhang, Y.; Lei, Z.; Olson, N.; Boyer, H. C.; Narayan, S.; Yee, L. D.; Green, H.; Cui, T. Increasing Isoprene Epoxydiol-to-Inorganic Sulfate Aerosol (IEPOX:$Sulf_{inorg}$) Ratio Results in Extensive Conversion of Inorganic Sulfate to Organosulfur Forms: Implications for Aerosol Physicochemical Properties. *Environ. Sci. Technol.* **2019**, DOI: 10.1021/acs.est.9b01019.

DOI: 10.1021/acsearthspacechem.9b00121
ACS Earth Space Chem. 2019, 3, 1260−1267